

Diffractive Electroproduction *

A. HEBECKER

Institut für Theoretische Physik der Universität Heidelberg
Philosophenweg 16, D-69120 Heidelberg, Germany

In these lectures, a simple introduction to the phenomenon of diffraction in deep inelastic scattering and its theoretical description is given. While the main focus is on the diffractive structure function F_2^D , some issues in diffractive vector meson production are also discussed.

1. Introduction

In the following, the term ‘diffractive electroproduction’ or ‘diffractive deep inelastic scattering (DIS)’ is used to characterize those processes in small- x DIS where, in spite of the high virtuality of the exchanged photon, the proton target remains intact or almost intact. Thus, the term is used synonymously with the expression ‘rapidity gap events in DIS’.

Historically, the term diffraction is derived from optics, where it describes the deflection of a beam of light and its decomposition into components with different frequencies. In high energy physics, it was originally used for small-angle elastic scattering of hadrons (Fig. 1a). If one of the hadrons, say the projectile, is transformed into a set of two or more final state particles, the process is called diffractive dissociation or inelastic diffraction. Good and Walker have pointed out that a particularly intuitive physical picture of such processes emerges if the projectile is described as a superposition $A + B$ of different components which scatter elastically off the target [1] (Fig. 1b). Since the corresponding elastic amplitude is different for each component, the outgoing beam will contain a new superposition $\alpha A + \beta B$ of these components and therefore, in general, new physical states. These are the dissociation products of the projectile.

Even at very high energy, the above processes are generically soft, i.e., the momentum transfer is small and the dissociation products have small p_{\perp} . Therefore, no immediate relation to perturbative QCD is apparent.

* lectures at the Cracow School of Theoretical Physics, XXXIX Course, Zakopane 1999

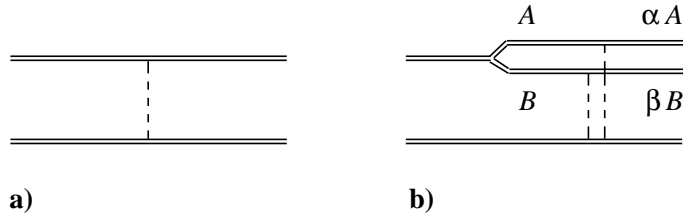


Figure 1: Elastic scattering (a) and diffractive dissociation (b) in the physical picture of Good and Walker [1].

In contrast to these soft processes, diffractive DIS is an example of hard diffraction, the hard scale being the virtuality Q^2 of the exchanged photon. However, this is not the first hard diffractive process that was observed. Hard diffraction was first investigated in diffractive jet production at the CERN $S\bar{p}p$ S collider in proton-antiproton collisions [2]. Although one of the hadrons escapes essentially unscathed, a high- p_\perp jet pair, which is necessarily associated with a high virtuality in the intermediate states, is produced in the central rapidity range (Fig. 2). The cross section of the process is parametrically unsuppressed relative to non-diffractive jet production. This seems to contradict a naïve partonic picture since the colour neutrality of the projectile is destroyed if one parton is removed to participate in the hard scattering. The interplay of soft and hard physics necessary to explain the effect provides one of the main motivations for the study of these ‘hard diffractive’ processes.

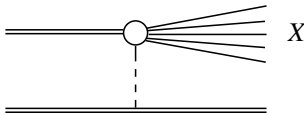


Figure 2: Diffractive dissociation in hadron-hadron collisions. If the diffractive final state X contains two high- p_\perp jets, the process is called diffractive jet production.

Here, the focus is on diffractive electroproduction, which is another example of a hard diffractive process. This process became experimentally viable with the advent of the electron-proton collider HERA (cf. [3]), where DIS at very small values of the Bjorken variable x can be studied. In the small- x or high-energy region, a significant fraction of the observed DIS events have a large rapidity gap between the photon and the proton fragmentation region [4, 5]. In contrast to the standard DIS process $\gamma^*p \rightarrow X$

(Fig. 3a), the relevant reaction reads $\gamma^*p \rightarrow XY$ (Fig. 3b), where X is a high-mass hadronic state and Y is the elastically scattered proton or a low-mass excitation of it. Again, these events are incompatible with the naïve picture of a partonic target and corresponding simple ideas about the colour flow. Naïvely, the parton struck by the virtual photon destroys the colour neutrality of the proton, a colour string forms between struck quark and proton remnant, and hadronic activity is expected throughout the detector. Nevertheless, the observed diffractive cross section is not power suppressed at high virtualities Q^2 with respect to standard DIS.

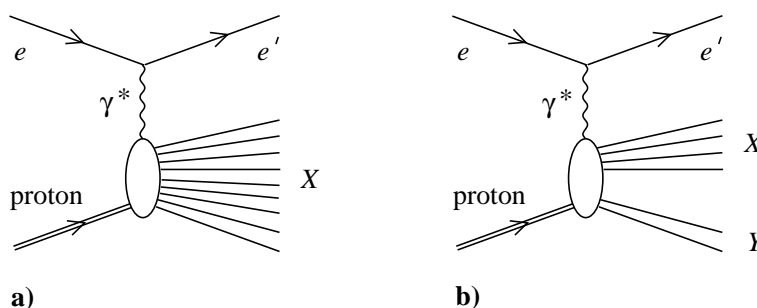


Figure 3: Inclusive (a) and diffractive (b) electroproduction.

These notes are organized as follows. In Sect. 2, the basic experimental observations and the diffractive structure function F_2^D are discussed. Section 3 describes the theory of F_2^D , emphasizing the semiclassical approach and its relation to the concept of diffractive parton distributions. In Sect. 4, some topics in diffractive meson production, in particular the factorization of the hard amplitude, are described. A brief summary is given in Sect. 5.

The reader may consult [6] for a more detailed review.

2. Basic observations and the diffractive structure function F_2^D

In this section, the kinematics of diffractive electroproduction at small x is explained in some detail, and the notation conventionally used for the description of this phenomenon is introduced. The main experimental observations are discussed, and the concept of the diffractive structure function, which is widely used in analyses of inclusive diffraction, is explained.

2.1. Kinematics

To begin, recall the conventional variables for the description of DIS. An electron with momentum k collides with a proton with momentum P . In neutral current processes, a photon with momentum q and virtuality

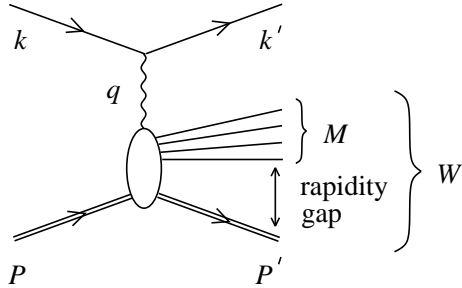


Figure 4: Diffractive electroproduction. The full hadronic final state with invariant mass W contains the elastically scattered proton and the diffractive state with invariant mass M .

$q^2 = -Q^2$ is exchanged, and the outgoing electron has momentum $k' = k - q$. In inclusive DIS, no questions are asked about the hadronic final state X_W , which is only known to have an invariant mass square $W^2 = (P + q)^2$. The Bjorken variable $x = Q^2/(Q^2 + W^2)$ characterizes, in the naïve parton model, the momentum fraction of the incoming proton carried by the quark that is struck by the virtual photon. If $x \ll 1$, which is the relevant region in the present context, Q is much smaller than the photon energy in the target rest frame. In this sense, the photon is almost real even though $Q^2 \gg \Lambda^2$ (where Λ is some soft hadronic scale). It is then convenient to think in terms of a high-energy γ^*p collision with centre-of-mass energy W .

Loosely speaking, diffraction is the subset of DIS characterized by a quasi-elastic interaction between virtual photon and proton. A particularly simple definition of diffraction is obtained by demanding that, in the γ^*p collision, the proton is scattered elastically. Thus, in diffractive events, the final state contains the scattered proton with momentum P' and a diffractive hadronic state X_M with mass M (see Fig. 4). Since diffractive events form a subset of DIS events, the total invariant mass of the outgoing proton and the diffractive state X_M is given by the standard DIS variable W .

The following parallel description of inclusive and diffractive DIS suggests itself.

In the former, virtual photon and proton collide to form a hadronic state X_W with mass W . The process can be characterized by the virtuality Q^2 and the scaling variable $x = Q^2/(Q^2 + W^2)$, the momentum fraction of the struck quark in the naïve parton model.

In the latter, a colour neutral cluster of partons is stripped off the proton. The virtual photon forms, together with this cluster, a hadronic state X_M with mass M . The process can be characterized by Q^2 , as above, and by a new scaling variable $\beta = Q^2/(Q^2 + M^2)$, the momentum fraction of this

cluster carried by the struck quark.

Since diffraction is a subprocess of inclusive DIS, the struck quark from the colour neutral cluster also carries a fraction x of the proton momentum. Therefore, the ratio $\xi = x/\beta$ characterizes the momentum fraction that the proton loses to the colour neutral exchange typical of an elastic reaction. This exchanged colour neutral cluster loses a momentum fraction β to the struck quark that absorbs the virtual photon. As expected, the product $x = \beta\xi$ is the fraction of the original proton's momentum carried by this struck quark. Since the name pomeron is frequently applied to whichever exchange with vacuum quantum numbers dominates the high-energy limit, many authors use the notation $x_P = \xi$, thus implying that the proton loses a momentum fraction ξ to the exchanged pomeron.

Therefore, x , Q^2 and β or, alternatively, x , Q^2 and ξ are the main kinematic variables characterizing diffractive DIS. A further variable, $t = (P - P')^2$, is necessary if the transverse momenta of the outgoing proton and the state X_M relative to the γ^*P axis are measured. Since the proton is a soft hadronic state, the value of $|t|$ is small in most events. The small momentum transferred by the proton also implies that $M \ll W$.

To see this in more detail, introduce light-cone co-ordinates $q_{\pm} = q_0 \pm q_3$ and $q_{\perp} = (q_1, q_2)$. It is convenient to work in a frame where the transverse momenta of the incoming particles vanish, $q_{\perp} = P_{\perp} = 0$. Let Δ be the momentum transferred by the proton, $\Delta = P - P'$, and $m_p^2 = P^2 = P'^2$ the proton mass squared. For forward scattering, $P'_{\perp} = 0$, the relation

$$t = \Delta^2 = \Delta_+ \Delta_- = -\xi^2 m_p^2 \quad (2.1)$$

holds. Since $\xi = (Q^2 + M^2)/(Q^2 + W^2)$, this means that small M implies small $|t|$ and vice versa. Note, however, that the value of $|t|$ is larger for non-forward processes, where $t = \Delta_+ \Delta_- - \Delta_{\perp}^2$.

So far, diffractive events have been characterized as those DIS events which contain an elastically scattered proton in their hadronic final state. An even more striking feature is the large gap of hadronic activity seen in the detector between the scattered proton and the diffractive state X_M . It will now be demonstrated that this feature, responsible for the alternative name 'rapidity gap events', is a direct consequence of the relevant kinematics.

Recall the definition of the rapidity y of a particle with momentum k ,

$$y = \frac{1}{2} \ln \frac{k_+}{k_-} = \frac{1}{2} \ln \frac{k_0 + k_3}{k_0 - k_3}. \quad (2.2)$$

This is a convenient quantity for the description of high-energy collisions along the z -axis. Massless particles moving along this axis have rapidity $-\infty$ or $+\infty$, while all other particles are characterized by some finite intermediate value of y .

In the centre-of-mass frame of the γ^*p collision, with the z -axis pointing in the proton beam direction, the rapidity of the incoming proton is given by $y_p = \ln(P_+/m_p)$. At small ξ , the rapidity of the scattered proton is approximately the same. This is to be compared with the highest rapidity y_{\max} of any of the particles in the diffractive state X_M . Since the total plus component of the 4-momentum of X_M is given by $(\xi - x)P_+$, and the pion, with mass m_π , is the lightest hadron, none of the particles in X_M can have a rapidity above $y_{\max} = \ln((\xi - x)P_+/m_\pi)$. Thus, a rapidity gap of size $\Delta y = \ln(m_\pi/(\xi - x)m_p)$ exists between the outgoing proton and the state X_M . For typical values of $\xi \sim 10^{-3}$ the size of this gap can be considerable.

Note, however, that the term ‘rapidity gap events’ was coined to describe the appearance of diffractive events in the HERA frame, i.e., a frame defined by the electron-proton collision axis. The rapidity in this frame is, in general, different from the photon-proton frame rapidity discussed above. Nevertheless, the existence of a gap surrounding the outgoing proton in the γ^*p frame clearly implies the existence of a similar gap in the ep frame. The exact size of the ep -frame rapidity gap follows from the specific event kinematics. The main conclusion so far is the kinematic separation of outgoing proton and diffractive state X_M in diffractive events with small ξ .

Without losing any of the qualitative results, the requirement of a final state proton P' can be replaced by the requirement of a low-mass hadronic state Y , well separated from the diffractive state X_M . In this case, the argument connecting elastically scattered proton and rapidity gap has to be reversed: the existence of a gap between X_M and Y becomes the distinctive feature of diffraction and, under certain kinematic conditions, the interpretation of Y as an excitation of the incoming proton, which is now *almost* elastically scattered, follows.

2.2. The main experimental observations

Rapidity gaps are expected even if in all DIS events a quark is knocked out of the proton leaving a coloured remnant. The reason for this is the statistical distribution of the produced hadrons, which results in a small yet finite probability for final states with little activity in any specified detector region. However, the observations described below are clearly inconsistent with this explanation of rapidity gap events.

More than 5% of DIS events at HERA were found to possess a rapidity gap [4, 5]. The analyses are based on the pseudo-rapidity $\eta = -\ln \tan(\theta/2)$, where θ is the angle of an outgoing particle relative to the beam axis. Pseudo-rapidity and rapidity are identical for massless particles; the difference between these two quantities is immaterial for the qualitative discussion below.

In the ZEUS analysis, a rapidity η_{\max} was defined as the maximum

rapidity of a calorimeter cluster in an event. A cluster was defined as an isolated set of adjacent cells with summed energy higher than 400 MeV. The measured η_{\max} distribution is shown in Fig. 5. (Note that the smallest detector angle corresponds to $\eta_{\max} = 4.3$; larger values are an artifact of the clustering algorithm.)

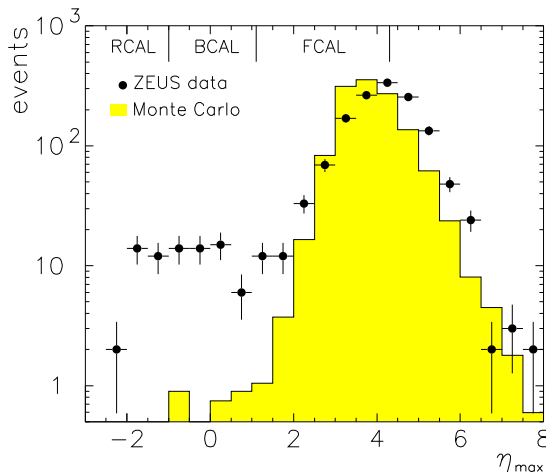


Figure 5: Distribution of η_{\max} , the maximum rapidity of a calorimeter cluster in an event, measured at HERA (figure from [4]).

To appreciate the striking qualitative signal of diffraction at HERA, the measured η_{\max} distribution has to be compared with naïve expectations based on a purely partonic picture of the proton. This is best done using a parton-model-based Monte Carlo event generator. The corresponding η_{\max} distribution, which is also shown in Fig. 5, is strongly suppressed at small η_{\max} . This qualitative behaviour is expected since the Monte Carlo (for more details see [4] and refs. therein) starts from a partonic proton, calculates the hard process and the perturbative evolution of the QCD cascade, and finally models the hadronization using the Lund string model (see, e.g., [7]). According to the Lund model, the colour string, which connects all final state partons and the coloured proton remnant, breaks up via $q\bar{q}$ pair creation, thus producing the observed mesons. The rapidities of these particles follow a Poisson distribution, resulting in an exponential suppression of large gaps.

It should be clear from the above discussion that this result is rather general and does not depend on the details of the Monte Carlo (note, however, the Monte Carlo based approach of [8], which allows for colour reconnection). QCD radiation tends to fill the rapidity range between the initially struck quark and the coloured proton remnant with partons. A colour string

connecting these partons is formed, and it is highly unlikely that a large gap emerges in the final state after the break-up of this string.

However, the data shows a very different behaviour. The expected exponential decrease of the event number with η_{\max} is observed only above $\eta_{\max} \simeq 1.5$; below this value a large plateau is seen. Thus, the naïve partonic description of DIS misses an essential qualitative feature of the data, namely, the existence of non-suppressed large rapidity gap events.

To give a more specific discussion of the diffractive event sample, it is necessary to define which events are to be called diffractive or rapidity gap events. It is clear from Fig. 5 that, on a qualitative level, this can be achieved by an η_{\max} cut separating the events of the plateau. The resulting qualitative features, observed both by the ZEUS [4] and H1 collaborations [5], are the following.

There exists a large rapidity interval where the η_{\max} distribution is flat. For high γ^*p energies W , the ratio of diffractive events to all DIS events is approximately independent of W . The Q^2 dependence of this ratio is also weak, suggesting a leading-twist contribution of diffraction to DIS. Furthermore, the diffractive mass spectrum is consistent with a $1/M^2$ distribution.

A number of additional remarks are in order. Note first that the observation of a flat η_{\max} distribution and of a $1/M^2$ spectrum are interdependent as long as masses and transverse momenta of final state particles are much smaller than M^2 . To see this, observe that the plus component of the most forward particle momentum and the minus component of the most backward particle momentum are largely responsible for the total invariant mass of the diffractive final state. This gives rise to the relation $dM^2/M^2 = d \ln M^2 \sim d\eta_{\max}$, which is equivalent to the desired result.

A significant contribution from exclusive vector meson production, e.g., the process $\gamma^*p \rightarrow \rho p$, is present in the rapidity gap event sample. A more detailed discussion of corresponding cross sections and of relevant theoretical considerations is given in Sect. 4.

2.3. Diffractive structure function

The diffractive structure function, introduced in [9] and first measured by the H1 collaboration [10], is a powerful concept for the analysis of data on diffractive DIS.

Recall the relevant formulae for inclusive DIS. The cross section for the process $ep \rightarrow eX$ can be calculated if the hadronic tensor,

$$W_{\mu\nu}(P, q) = \frac{1}{4\pi} \sum_X \langle P | j_\nu^\dagger(0) | X \rangle \langle X | j_\mu(0) | P \rangle (2\pi)^4 \delta^4(q + P - p_X), \quad (2.3)$$

is known. Here j is the electromagnetic current, and the sum is over all hadronic final states X . Because of current conservation, $q \cdot W = W \cdot q = 0$, the tensor can be decomposed according to

$$W_{\mu\nu}(P, q) = \left(g_{\mu\nu} - \frac{q_\mu q_\nu}{q^2} \right) W_1(x, Q^2) + \left(P_\mu + \frac{1}{2x} q_\mu \right) \left(P_\nu + \frac{1}{2x} q_\nu \right) W_2(x, Q^2). \quad (2.4)$$

The data is conveniently analysed in terms of the two structure functions

$$F_2(x, Q^2) = (P \cdot q) W_2(x, Q^2) \quad (2.5)$$

$$F_L(x, Q^2) = (P \cdot q) W_2(x, Q^2) - 2x W_1(x, Q^2). \quad (2.6)$$

Introducing the ratio $R = F_L/(F_2 - F_L)$, the electron-proton cross section can be written as

$$\frac{d^2 \sigma_{ep \rightarrow eX}}{dx dQ^2} = \frac{4\pi\alpha_{\text{em}}^2}{xQ^4} \left\{ 1 - y + \frac{y^2}{2[1 + R(x, Q^2)]} \right\} F_2(x, Q^2), \quad (2.7)$$

where $y = Q^2/sx$, and s is the electron-proton centre-of-mass energy squared. In the naïve parton model or at leading order in α_s in QCD, the longitudinal structure function $F_L(x, Q^2)$ vanishes, and $R = 0$. Since R corresponds to the ratio of longitudinal and transverse virtual photon cross sections, σ_L/σ_T , it is always positive, and the corrections associated with a non-zero R are small at low values of y .

In diffraction, the two additional kinematic variables ξ and t are present. However, no additional independent 4-vector is introduced as long as the measurement is inclusive with respect to the azimuthal angle of the scattered proton. Therefore, the decomposition in Eq. (2.4) remains valid, and the two diffractive structure functions $F_{2,L}^{D(4)}(x, Q^2, \xi, t)$ can be defined. The diffractive cross section reads

$$\frac{d^2 \sigma_{ep \rightarrow epX_M}}{dx dQ^2 d\xi dt} = \frac{4\pi\alpha_{\text{em}}^2}{xQ^4} \left\{ 1 - y + \frac{y^2}{2[1 + R^{D(4)}(x, Q^2, \xi, t)]} \right\} F_2^{D(4)}(x, Q^2, \xi, t), \quad (2.8)$$

where $R^D = F_L^D/(F_2^D - F_L^D)$. In view of the limited precision of the data, the dominance of the small- y region, and the theoretical expectation of the smallness of F_L^D , the corrections associated with a non-zero value of R^D are neglected in the following.

A more inclusive and experimentally more easily accessible quantity can be defined by performing the t integration,

$$F_2^{D(3)}(x, Q^2, \xi) = \int dt F_2^{D(4)}(x, Q^2, \xi, t). \quad (2.9)$$

The main qualitative features of diffractive electroproduction, already discussed in the previous section, become particularly apparent if the functional form of $F_2^{D(3)}$ is considered (cf. the data in Figs. 13 and 14 in Sect. 3). The β and Q^2 dependence of $F_2^{D(3)}$ is relatively flat. This corresponds to the observations discussed earlier that diffraction is a leading twist effect and that the mass distribution is consistent with a $1/M_X^2$ spectrum. The energy dependence of diffraction is such that $\xi F_2^{D(3)}(\xi, \beta, Q^2)$ slowly grows as $\xi \rightarrow 0$. This growth and its possible relation to the growth of inclusive structure functions at small x and to the growth of elastic cross sections at high energy is one of the most interesting aspects of diffraction (see also [11]).

3. Theoretical approaches to F_2^D

To understand qualitatively how leading twist diffraction in DIS comes about, it is simplest to work in the target rest frame. Diffraction means that a hadronic fluctuation of the energetic virtual photon scatters off the target proton without exchanging colour. One can then expect the photon and the proton to fragment independently, leading to a rapidity gap event.

A particularly simple physical picture is provided by the aligned jet model of Bjorken and Kogut [12]. In terms of the QCD degrees of freedom, a closely related formulation of diffraction was given with the two-gluon exchange calculations of Nikolaev and Zakharov [13]. Since the t channel colour singlet exchange is not hard in the bulk of the cross section underlying F_2^D , the exchange of more than two gluons is not suppressed. This can be systematically treated in the semiclassical approach [14, 15].

In the Breit frame, where the target proton is fast, diffraction was historically described as DIS off a pomeron [16, 17]. A more general, QCD based concept treating diffraction from a Breit frame point of view are the diffractive parton distributions [18, 19]. As will be discussed in more detail below, the semiclassical approach provides a convenient framework in which one can intuitively understand how diffractive parton distributions emerge in a target rest calculation.

3.1. Aligned jet model

A very simple argument why, even at very high photon virtualities, diffractive DIS is largely a soft process was presented by Bjorken and Kogut in the framework of their aligned jet model [12].

The underlying physical picture is based on vector meson dominance ideas. The incoming photon fluctuates into a hadronic state with mass M , which then collides with the target (see Fig. 6a). The corresponding cross

section for transverse photon polarization is estimated by

$$\frac{d\sigma_T}{dM^2} \sim \frac{dP(M^2)}{dM^2} \cdot \sigma(M^2), \quad (3.1)$$

where the probability for the photon to develop a fluctuation with mass M is given by

$$dP(M^2) \sim \frac{M^2 dM^2}{(M^2 + Q^2)^2}, \quad (3.2)$$

and $\sigma(M^2)$ is the cross section for this fluctuation to scatter off the target. The above expression for $dP(M^2)$ is most easily motivated in the framework of old-fashioned perturbation theory, where the energy denominator of the amplitude is proportional to the off-shellness of the hadronic fluctuation, $Q^2 + M^2$. If this is the only source for a Q^2 dependence, the numerator factor M^2 is necessary to obtain a dimensionless expression.

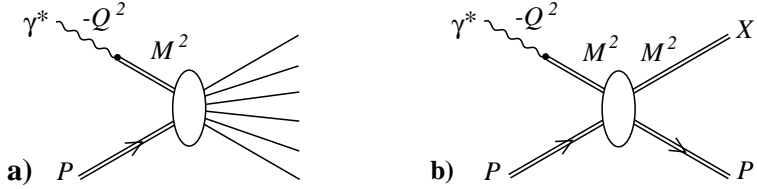


Figure 6: Vector meson dominance inspired picture of inclusive (a) and diffractive (b) electroproduction.

Bjorken and Kogut assume that, for large M^2 , the intermediate hadronic state typically contains two jets and that $\sigma(M^2)$ is suppressed for configurations with high p_\perp (the latter effect being now known under the name of colour transparency). Consider hadronic fluctuations with a certain M^2 , which, in their respective rest frames, are realized by two back-to-back jets. Under the assumption that the probability distribution of the direction of the jet axis is isotropic, simple geometry implies that aligned configurations, defined by $p_\perp^2 < \Lambda^2$ (where Λ^2 is a soft hadronic scale), are suppressed by Λ^2/M^2 . If only such configurations are absorbed with a large, hadronic cross section, the relations $\sigma(M^2) \sim 1/M^2$ and

$$\frac{d\sigma_T}{dM^2} \sim \frac{1}{(M^2 + Q^2)^2} \quad (3.3)$$

follow. Thus, the above cross section can be interpreted as the total high-energy cross section of target proton and aligned jet fluctuation of the photon, i.e., of two soft hadronic objects. Therefore, a similar elastic cross section is expected, $\sigma_T^D \sim \sigma_T$ (cf. Fig. 6b). The resulting diffractive structure

function reads

$$F_2^{D(3)}(\xi, \beta, Q^2) \sim \beta/\xi. \quad (3.4)$$

It is interesting that the very simple arguments outlined above capture two important features of the HERA data: the leading-twist nature of diffraction and the approximate $1/\xi$ behaviour of F_2^D .

3.2. Two-gluon exchange

The simplest way to formulate the above intuitive picture, where a hadronic fluctuation of the photon scatters off the proton, in perturbative QCD is via two-gluon exchange. At leading order, the photon fluctuates in a $q\bar{q}$ pair and two gluons forming a colour singlet are exchanged in the t channel (see Fig. 7). A corresponding calculation was first performed by Nikolaev and Zakharov [13], where the probability for the photon to fluctuate in a $q\bar{q}$ pair was described by the square of the light-cone wave function of the photon. The scattering of the $q\bar{q}$ pair off the proton was parametrized using the dipole cross section $\sigma(\rho)$, where ρ is the transverse distance between quark and antiquark when they hit the target. Here, the corresponding calculations will not be described (see, however, the recent review of diffraction [20] emphasizing two-gluon exchange). Note that two-gluon exchange results can be recovered from the semiclassical calculation described below if a Taylor expansion in the external colour field is performed.

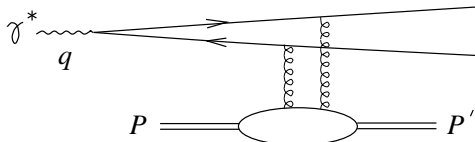


Figure 7: Diffractive electroproduction in the two-gluon exchange model.

Gluon radiation, i.e., the fluctuation of the incoming photon in a $q\bar{q}g$ state was considered in [21].

For further interesting work related to the two-gluon exchange approximation for F_2^D see, e.g., [22–24] (cf. [25] for new developments in the BFKL resummation method). Note also the discussion of diffractive processes in the colour-dipole approach [26] and the combined analysis of diffractive and inclusive DIS in this framework [27].

The main shortcoming of the two-gluon approach is the lacking justification of perturbation theory. As should be clear from the aligned jet model and as will be discussed in a more technical way below, the diffractive kinematics is such that the t channel colour singlet exchange does not

feel the hard scale of the initial photon. Thus, more than two gluons can be exchanged without suppression by powers of α_s .

Note that this is different in certain more exclusive processes, such as vector meson production, where it has been shown that the dynamics of the t channel exchange is governed by a hard, perturbative scale (cf. Sect. 4).

3.3. Semiclassical approach

In this approach, the interaction with the target is modelled as the scattering off a superposition of soft target colour fields, which, in the high-energy limit, can be calculated in the eikonal approximation [28]. Diffraction occurs if both the target and the partonic fluctuation of the photon remain in a colour singlet state.

The amplitude for an energetic parton to scatter off a given colour field configuration is a fundamental building block in the semiclassical approach. The essential assumptions are the softness and localization of the colour field and the very large energy of the scattered parton.

The relevant physical situation is depicted in Fig. 8, where the blob symbolizes the target colour field configuration. Consider first the case of a scalar quark that is minimally coupled to the gauge field via the Lagrangian

$$\mathcal{L}_{\text{scalar}} = (D_\mu \Phi)^* (D^\mu \Phi) \quad \text{with} \quad D_\mu = \partial_\mu + igA_\mu. \quad (3.5)$$

In the high-energy limit, where the plus component of the quark momentum becomes large, the amplitude of Fig. 8 then reads

$$i2\pi\delta(k'_0 - k_0)T = 2\pi\delta(k'_0 - k_0)2k_0 \left[\tilde{U}(k'_\perp - k_\perp) - (2\pi)^2\delta^2(k'_\perp - k_\perp) \right]. \quad (3.6)$$

It is normalized as is conventional for scattering processes off a fixed target. The expression in square brackets is the Fourier transform of the impact parameter space amplitude, $U(x_\perp) - 1$, where

$$U(x_\perp) = P \exp \left(-\frac{ig}{2} \int_{-\infty}^{\infty} A_-(x_+, x_\perp) dx_+ \right) \quad (3.7)$$

is the non-Abelian eikonal factor. The unit matrix $1 \in SU(N_c)$, with N_c the number of colours, subtracts the field independent part, and the path ordering operator P sets the field at smallest x_+ to the rightmost position.

This formula was derived by many authors [28–30]. A derivation based on the summation of diagrams of the type shown in Fig. 9, is given in the Appendix of [6].

The amplitude of Eq. (3.6) is easily generalized to the case of a spinor quark or an energetic gluon. In the the high-energy limit, helicity-flip or polarization-flip contributions are suppressed.

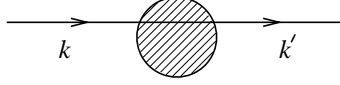


Figure 8: Scattering of a quark off the target colour field.

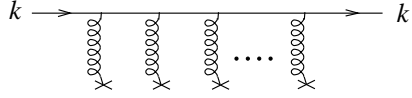


Figure 9: Typical diagrammatic contribution to the eikonal amplitude, Eq. (3.6). Attachments of gluon lines with crosses correspond to vertices at which the classical external field appears.

The eikonal approximation can be used for the calculation of the amplitude for $q\bar{q}$ pair production off a given target colour field [14]. Both diffractive and inclusive cross sections are obtained from the same calculation, diffraction being defined by the requirement of colour neutrality of the produced pair.

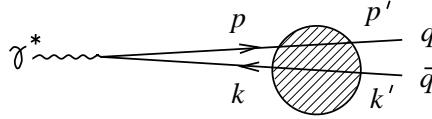


Figure 10: Electroproduction of a $q\bar{q}$ pair off the target colour field.

The process is illustrated in Fig. 10. The corresponding T matrix element has three contributions, $T = T_{q\bar{q}} + T_q + T_{\bar{q}}$, where $T_{q\bar{q}}$ corresponds to both the quark and antiquark interacting with the field, while T_q and $T_{\bar{q}}$ correspond to only one of the partons interacting with the field.

Let $V_q(p', p)$ and $V_{\bar{q}}(k', k)$ be the effective vertices for an energetic quark and antiquark interacting with a soft gluonic field. For quarks with charge e , one has

$$i2\pi\delta(k'_0 + k_0 - q_0)T_{q\bar{q}} \quad (3.8)$$

$$= ie \int \frac{d^4k}{(2\pi)^4} \bar{u}_{s'}(p')V_q(p', p) \frac{i}{\not{p}' - m} \not{\epsilon}(q) \frac{i}{-\not{k} - m} V_{\bar{q}}(k, k')v_{r'}(k'),$$

where $q = p + k$ by momentum conservation, $\epsilon(q)$ is the polarization vector of the incoming photon, and r', s' label the spins of the outgoing quarks.

The propagators in Eq. (3.8) can be treated in a high-energy approximation. In a co-ordinate system where the photon momentum is directed along the z -axis, the large components are p_+ and k_+ . It is convenient to introduce, for each vector k , a vector \bar{k} whose minus component satisfies the mass shell condition, $\bar{k}_- = (k_\perp^2 + m^2)/k_+$, while the other components are identical to those of k . The propagators in Eq. (3.8) can be rewritten according to

$$\frac{1}{\not{p} - m} = \frac{\sum_s u_s(\bar{p})\bar{u}_s(\bar{p})}{p^2 - m^2} + \frac{\gamma_+}{2p_+} \quad (3.9)$$

and an analogous identity for the propagator with momentum k . In the high-energy limit, the term proportional to γ_+ in Eqs. (3.9) can be dropped.

After inserting Eqs. (3.9) into Eq. (3.8), the relation

$$\bar{u}_{s'}(p')V_q(p', p)u_s(p) = 2\pi\delta(p'_0 - p_0)2p_0 \left[\tilde{U}(p'_\perp - p_\perp) - (2\pi)^2\delta^2(p'_\perp - p_\perp) \right] \delta_{ss'}, \quad (3.10)$$

which corresponds to Eq. (3.6), is applied. The vertex $V_{\bar{q}}(k, k')$ is treated analogously. Writing the loop integration as $d^4k = (1/2)dk_+dk_-d^2k_\perp$ and using the approximation $\delta(l_0) \simeq 2\delta(l_+)$ for the energy δ -functions, the k_+ integration becomes trivial. The k_- integral is done by closing the integration contour in the upper or lower half of the complex k_- plane. The result reads

$$T_{q\bar{q}} = -\frac{ie}{4\pi^2} q_+ \int d^2k_\perp \frac{\alpha(1-\alpha)}{N^2 + k_\perp^2} \bar{u}_{s'}(\bar{p})\not{q}v_{r'}(\bar{k}) \times \left[\tilde{U}(p'_\perp - p_\perp) - (2\pi)^2\delta^2(p'_\perp - p_\perp) \right] \left[\tilde{U}^\dagger(k_\perp - k'_\perp) - (2\pi)^2\delta^2(k'_\perp - k_\perp) \right] \quad (3.11)$$

where $p'_+ = (1-\alpha)q_+$, $k'_+ = \alpha q_+$, $N^2 = \alpha(1-\alpha)Q^2 + m^2$. Thus, α and $1-\alpha$ characterize the fractions of the photon momentum carried by the two quarks, while $(N^2 + k_\perp^2)$ measures the off-shellness of the partonic fluctuation before it hits the target. In the following we set $m = 0$.

Adding T_q and $T_{\bar{q}}$ and introducing the fundamental function

$$W_{x_\perp}(y_\perp) = U(x_\perp)U^\dagger(x_\perp + y_\perp) - 1, \quad (3.12)$$

which encodes all the information about the external field, the complete amplitude can eventually be given in the form

$$T = -\frac{ie}{4\pi^2} q_+ \int d^2k_\perp \frac{\alpha(1-\alpha)}{N^2 + k_\perp^2} \bar{u}_{s'}(\bar{p})\not{q}v_{r'}(\bar{k}) \int_{x_\perp} e^{-i\Delta_\perp x_\perp} \tilde{W}_{x_\perp}(k'_\perp - k_\perp), \quad (3.13)$$

where \tilde{W}_{x_\perp} is the Fourier transform of $W_{x_\perp}(y_\perp)$ with respect to y_\perp , and $\Delta_\perp = k'_\perp + p'_\perp$ is the total transverse momentum of the final $q\bar{q}$ state.

From the above amplitude, the transverse and longitudinal virtual photon cross sections are calculated in a straightforward manner using the explicit formulae for $\bar{u}_{s'}(\bar{p})\not{\epsilon}(q)v_{r'}(\bar{k})$. Summing over all $q\bar{q}$ colour combinations, as appropriate for the inclusive DIS cross section, the following result is obtained,

$$\frac{d\sigma_L}{d\alpha dk_{\perp}^{\prime 2}} = \frac{2e^2 Q^2}{(2\pi)^6} (\alpha(1-\alpha))^2 \int_{x_{\perp}} \left| \int d^2 k_{\perp} \frac{\tilde{W}_{x_{\perp}}(k'_{\perp} - k_{\perp})}{N^2 + k_{\perp}^2} \right|^2, \quad (3.14)$$

$$\frac{d\sigma_T}{d\alpha dk_{\perp}^{\prime 2}} = \frac{e^2}{2(2\pi)^6} (\alpha^2 + (1-\alpha)^2) \int_{x_{\perp}} \left| \int d^2 k_{\perp} \frac{k_{\perp} \tilde{W}_{x_{\perp}}(k'_{\perp} - k_{\perp})}{N^2 + k_{\perp}^2} \right|^2 \quad (3.15)$$

The contraction of the colour indices of the two W matrices is implicit.

An explicit calculation shows (see, e.g., [6]) that the leading contributions at high Q^2 are

$$\sigma_L = \frac{e^2}{6\pi^2 Q^2} \int_{x_{\perp}} |\partial_{\perp} W_{x_{\perp}}(0)|^2 \quad (3.16)$$

and

$$\begin{aligned} \sigma_T &= \frac{e^2}{6\pi^2 Q^2} \left(\ln \frac{Q^2}{\mu^2} - 1 \right) \int_{x_{\perp}} |\partial_{\perp} W_{x_{\perp}}(0)|^2 \quad (3.17) \\ &+ \frac{e^2}{(2\pi)^6} \int_0^{\mu^2/Q^2} d\alpha \int dk_{\perp}^{\prime 2} \int_{x_{\perp}} \left| \int d^2 k_{\perp} \frac{k_{\perp} \tilde{W}_{x_{\perp}}(k'_{\perp} - k_{\perp})}{N^2 + k_{\perp}^2} \right|^2, \end{aligned}$$

where $\Lambda^2 \ll \mu^2 \ll Q^2$.

The resulting physical picture can be summarized as follows. For longitudinal photon polarization, the produced $q\bar{q}$ pair has small transverse size and shares the photon momentum approximately equally. Only the small distance structure of the target colour field, characterized by the quantity $|\partial_{\perp} W_{x_{\perp}}(0)|^2$, is tested. For transverse photon polarization, an additional leading twist contribution comes from the region where α or $1-\alpha$ is small and $k_{\perp}^{\prime 2} \sim \Lambda^2$. In this region, the $q\bar{q}$ pair penetrating the target has large transverse size, and the large distance structure of the target colour field, characterized by the function $W_{x_{\perp}}(y_{\perp})$ at large y_{\perp} , is tested. This physical picture, known as the aligned jet model, was introduced in [12] on a qualitative level and was used more recently for a quantitative discussion of small- x DIS in [13].

Diffraction cross sections are now derived by introducing a colour singlet projector into the underlying amplitude, i.e., by the substitution

$$\text{tr} \left(W_{x_{\perp}}(y_{\perp}) W_{x_{\perp}}^{\dagger}(y'_{\perp}) \right) \rightarrow \frac{1}{N_c} \text{tr} W_{x_{\perp}}(y_{\perp}) \text{tr} W_{x_{\perp}}^{\dagger}(y'_{\perp}) \quad (3.18)$$

in Eqs. (3.14) and (3.15). This change of the colour structure has crucial consequences.

Firstly, the longitudinal cross section vanishes at leading twist (cf. Eq. (3.16)) since the derivative $\partial_{\perp} W_{x_{\perp}}(0)$ is in the Lie-algebra of $SU(N_c)$, and therefore $\text{tr} \partial_{\perp} W_{x_{\perp}}(0) = 0$.

Secondly, for the same reason the $\ln Q^2$ term in the transverse cross section, given by Eq. (3.17), disappears. The whole cross section is dominated by the endpoints of the α integration, i.e., the aligned jet region. At leading order in $1/Q^2$, the diffractive cross sections read

$$\sigma_L^D = 0 \tag{3.19}$$

$$\sigma_T^D = \frac{e^2}{(2\pi)^6 N_c} \int_0^{\infty} d\alpha \int dk_{\perp}'^2 \int_{x_{\perp}} \left| \int d^2 k_{\perp} \frac{k_{\perp} \text{tr} \tilde{W}_{x_{\perp}}(k'_{\perp} - k_{\perp})}{N^2 + k_{\perp}^2} \right|^2. \tag{3.20}$$

The cutoff of the α integration, μ^2/Q^2 , has been dropped since, due to the colour singlet projection, the integration is automatically dominated by the soft endpoint.

In summary, the leading-twist cross section for small- x DIS receives contributions from both small- and large-size $q\bar{q}$ pairs, the latter corresponding to aligned jet configurations. The requirement of colour neutrality in the final state suppresses the small-size contributions. Thus, leading twist diffraction is dominated by the production of pairs with large transverse size testing the non-perturbative large-distance structure of the target colour field.

3.4. Diffractive parton distributions

The basic theoretical ideas are due to Trentadue and Veneziano, who proposed to parametrize semi-inclusive hard processes in terms of ‘fracture functions’ [18], and to Berera and Soper, who defined similar quantities for the case of hard diffraction [19] and coined the term ‘diffractive parton distributions’. The following discussion is limited to the latter, more specialized framework.

Recall first that a conventional parton distribution $f_i(y)$ describes the probability of finding, in a fast moving proton, a parton i with momentum fraction y .

In short, diffractive parton distributions are conditional probabilities. A diffractive parton distribution $df_i^D(y, \xi, t)/d\xi dt$ describes the probability of finding, in a fast moving proton, a parton i with momentum fraction y , under the additional requirement that the proton remains intact while being scattered with invariant momentum transfer t and losing a small fraction ξ of its longitudinal momentum. Thus, the corresponding γ^*p cross section

can be written as [31]

$$\frac{d\sigma(x, Q^2, \xi, t)^{\gamma^* p \rightarrow p' X}}{d\xi dt} = \sum_i \int_x^\xi dy \hat{\sigma}(x, Q^2, y)^{\gamma^* i} \left(\frac{df_i^D(y, \xi, t)}{d\xi dt} \right), \quad (3.21)$$

where $\hat{\sigma}(x, Q^2, y)^{\gamma^* i}$ is the total cross section for the scattering of a virtual photon characterized by x and Q^2 and a parton of type i carrying a fraction y of the proton momentum. The above factorization formula holds in the limit $Q^2 \rightarrow \infty$ with x , ξ and t fixed.

At leading order and in the case of transverse photon polarization, only the quark distribution contributes. For one quark flavour with one unit of electric charge, the well-known partonic cross section reads

$$\hat{\sigma}_T(x, Q^2, y)^{\gamma^* q} = \frac{\pi e^2}{Q^2} \delta(1 - y/x), \quad (3.22)$$

giving rise to the diffractive cross section

$$\frac{d\sigma(x, Q^2, \xi, t)^{\gamma^* p \rightarrow p' X}}{d\xi dt} = \frac{2\pi e^2}{Q^2} \frac{x df_q^D(x, \xi, t)}{d\xi dt}, \quad (3.23)$$

where the factor 2 is introduced to account for the antiquark contribution.

As in inclusive DIS, there are infrared divergences in the partonic cross sections and ultraviolet divergences in the parton distributions. They are conveniently renormalized with the $\overline{\text{MS}}$ prescription, which introduces the scale μ as a further argument. The distribution functions then read $f_i(x, \mu^2)$ and $df_i^D(x, \xi, t, \mu^2)/d\xi dt$ in the inclusive and diffractive case respectively.

Accordingly, Eq. (3.21) has to be read in the $\overline{\text{MS}}$ scheme, with a μ dependence appearing both in the parton distributions and in the partonic cross sections. The claim that Eq. (3.21) holds to all orders implies that these μ dependences cancel, as is well known in the case of conventional parton distributions. Since the partonic cross sections are the same in both cases, the diffractive distributions obey the usual Altarelli-Parisi evolution equations,

$$\frac{d}{d(\ln \mu^2)} \frac{df_i^D(x, \xi, t, \mu^2)}{d\xi dt} = \sum_j \int_x^\xi \frac{dy}{y} P_{ij}(x/y) \frac{df_j^D(y, \xi, t, \mu^2)}{d\xi dt}. \quad (3.24)$$

with the ordinary splitting functions $P_{ij}(x/y)$.

Thus, for the analysis of diffractive DIS, it is essential to gain confidence in the validity of the factorization formula Eq. (3.21). Berera and Soper first pointed out [31] that such a factorization proof could be designed along the lines of related results for other QCD processes (see [32] for a review).

Proofs were given by Grazzini, Trentadue and Veneziano in the framework of a simple scalar model [33] and by Collins in full QCD [34].

The concept of diffractive parton distributions is more rigorous but less predictive than the older, widely used method of parton distributions of the pomeron [16, 17, 35]. This method originates in the observation that diffractive DIS can be understood as the soft high-energy scattering of the hadronic fluctuation of the photon and the target proton. Since a large sample of hadronic cross sections can be consistently parametrized using the concept of the Donnachie-Landshoff or soft pomeron [36], it is only natural to assume that this concept can also be used in the present case. A more direct way of applying the concept of the soft pomeron to the phenomenon of hard diffraction was suggested by Ingelman and Schlein in the context of diffractive jet production in hadronic collisions [16]. Their idea of a partonic structure of the pomeron, which can be tested in hard processes, applies to the case of diffractive DIS as well [17]. Essentially, one assumes that the pomeron can, like a real hadron, be characterized by a parton distribution. This distribution factorizes from the pomeron trajectory and the pomeron-proton vertex, which are both obtained from the analysis of purely soft hadronic reactions. The above non-trivial assumptions, which have not been derived from QCD, are often referred to as ‘Regge hypothesis’ or ‘Regge factorization’.

3.5. Diffractive parton distributions in the semiclassical approach

It will be shown how the semiclassical calculation can be factorized into hard and soft part and how a model for diffractive parton densities naturally arises from the soft part of the semiclassical calculation [37].

For simplicity, consider the fluctuation of the photon into a set of scalar partons which interact independently with the proton colour field (see Fig. 11).

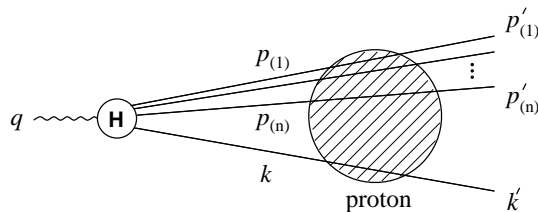


Figure 11: Hard diffractive process in the proton rest frame. The soft parton with momentum k is responsible for the leading twist behaviour of the cross section.

Assume furthermore that the transverse momenta $p'_{(j)\perp}$ ($j = 1 \dots n$) are hard, i.e. $\mathcal{O}(Q)$. A leading twist contribution to diffraction can arise only if the transverse momentum of the remaining parton is small, $k'_\perp \sim \Lambda_{\text{QCD}}$.

The standard cross section formula for the scattering off a static external field reads

$$d\sigma = \frac{1}{2q_0} |T|^2 2\pi\delta(q_0 - q'_0) dX^{(n+1)}, \quad \text{where } q' = k' + \sum p'_{(j)}. \quad (3.25)$$

All momenta are given in the proton rest frame, T is the amplitude corresponding to Fig. 11, and $dX^{(n+1)}$ is the usual phase space element for $n+1$ particles.

The colour rotation experienced by each parton penetrating the external field is described by an eikonal factor. The resulting amplitude is given by

$$i 2\pi\delta(q_0 - q'_0) T = \int T_H \left(\frac{i}{k^2} 2\pi\delta(k'_0 - k_0) 2k_0 \tilde{U}(k'_\perp - k_\perp) \right) \\ \times \prod_j \left(\frac{i}{p_{(j)}^2} 2\pi\delta(p'_{(j)0} - p_{(j)0}) 2p_{(j)0} \tilde{U}(p'_{(j)\perp} - p_{(j)\perp}) \frac{d^4 p_{(j)}}{(2\pi)^4} \right), \quad (3.26)$$

where T_H stands for the hard part of the diagram in Fig. 11.

The integrations over the light-cone components $p_{(j)+}$ can be performed using the energy δ -functions. The $p_{(j)-}$ -integrations are performed by picking up the poles of the propagators $1/p_{(j)}^2$. Since the external field is smooth and T_H is dominated by the hard scale, $n-1$ of the n transverse momentum integrations can be performed trivially. This is not the case for the last integration which will necessarily be sensitive to the small off-shellness k^2 . However, the $n-1$ performed integrations ensure that the eikonal factors associated with the high- p_\perp partons are evaluated at the same transverse position. The resulting colour structure of the amplitude, after projection on a colour singlet final state, involves the trace of $\tilde{W}_{x_\perp}(y_\perp)$ (cf. Eq. 3.12). It is intuitively clear that only two eikonal factors are present since the high- p_\perp partons are close together in transverse space. They are colour rotated like a single parton.

Under the further assumption that final state momenta of the high- p_\perp partons are not resolved on the soft scale, the following result is derived,

$$\frac{d\sigma}{dX^{(n+1)}} = \frac{k_0^2 |T_H|^2}{\pi q_0 N_c} \int_{x_\perp} \left| \int_{k_\perp} \frac{\text{tr}[\tilde{W}_{x_\perp}(k'_\perp - k_\perp)]}{k^2} \right|^2 \delta^2(\sum p_{(j)\perp}) \delta(q_0 - q'_0). \quad (3.27)$$

In this expression the non-perturbative input encoded in the Fourier transform \tilde{W} is totally decoupled from the hard momenta that dominate T_H .

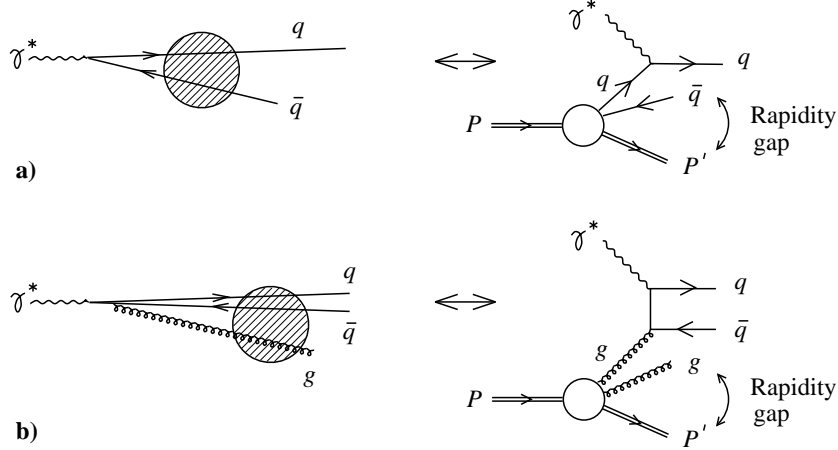


Fig. 12. Diffractive DIS in the proton rest frame (left) and the Breit frame (right); asymmetric quark fluctuations correspond to diffractive quark scattering, asymmetric gluon fluctuations to diffractive boson-gluon fusion.

The squared amplitude $|T_H|^2$ in Eq. (3.27) can be expressed through the partonic cross section $\hat{\sigma}(x, Q^2, y)$. In Fig. 11 this corresponds to the interpretation of the line labelled by k as an incoming line for the hard process. The cross section differential in ξ takes the form

$$\frac{d\sigma}{d\xi} = \int_x^\xi dy \hat{\sigma}(x, Q^2, y) \left(\frac{df_s(y, \xi)}{d\xi} \right). \quad (3.28)$$

Introducing the variable $b = y/\xi$ the diffractive parton density for scalars (integrated over t) reads

$$\frac{df_s(y, \xi)}{d\xi} = \frac{1}{\xi^2} \left(\frac{b}{1-b} \right) \int \frac{d^2 k'_\perp (k'_\perp)^2}{(2\pi)^4 N_c} \int_{x_\perp} \left| \int \frac{d^2 k_\perp}{(2\pi)^2} \frac{\text{tr}[\tilde{W}_{x_\perp}(k'_\perp - k_\perp)]}{k'_\perp{}^2 b + k_\perp{}^2 (1-b)} \right|^2. \quad (3.29)$$

Analogous considerations with spinor and vector partons result in the same factorizing result, but with different distribution functions.

The physical picture emerging from the above semiclassical calculation of diffractive parton distributions is illustrated in Fig. 12. In the Breit frame, leading order diffractive DIS is most naturally described by photon-quark scattering, with the quark coming from the diffractive parton distribution of the target hadron. This is illustrated on the r.h. side of Fig. 12a. Identifying the leading twist part of the $q\bar{q}$ pair production cross section (l.h. side of Fig. 12a) with the result of the conventional partonic calculation (r.h. side of Fig. 12a), the diffractive quark distribution of the target is expressed in terms of the color field dependent function given in Eq. (3.12).

Similarly, the cross section for the color singlet production of a $q\bar{q}g$ state (l.h. side of Fig. 12b) is identified with the boson-gluon fusion process based on the diffractive gluon distribution of the target (r.h. side of Fig. 12b). This allows for the calculation of the diffractive gluon distribution in terms of a function similar to Eq. (3.12) but with the U matrices in the adjoint representation.

In the semiclassical approach, the cross sections for inclusive DIS are obtained from the same calculations as in the diffractive case where, however, the color singlet condition for the final state parton configuration is dropped. As a result, the $q\bar{q}$ production cross section (cf. the l.h. side of Fig. 12a) receives contributions from both the aligned jet and the high- p_{\perp} region. In the latter, the logarithmic dp_{\perp}^2/p_{\perp}^2 integration gives rise to a $\ln Q^2$ term in the full cross section.

In the leading order partonic analysis, the full cross section is described by photon-quark scattering. The gluon distribution is responsible for the scaling violations at small x , $\partial F_2(x, Q^2)/\partial \ln Q^2 \sim xg(x, Q^2)$. Thus, the semiclassical result for $q\bar{q}$ production, with its $\ln Q^2$ contribution, is sufficient to calculate both the inclusive quark and the inclusive gluon distribution. The results are again expressed in terms of the function in Eq. (3.12) where now the color trace is taken *after* the two W matrices (corresponding to the amplitude and its complex conjugate) have been multiplied.

To obtain explicit formulae for the above parton distributions, a model for the averaging over the color fields has to be introduced. Such models are provided, e.g., by the non-perturbative stochastic vacuum [38] or by the perturbative small dipoles of [39]. The large hadron model [40], on which the following analysis is based, has the advantage of justifying the Fock space expansion of the photon wave function while being intrinsically non-perturbative as far as the t channel colour exchange is concerned.

In the case of a very large hadronic target [40] (see also [41]), even in the aligned jet region, the transverse separation of the $q\bar{q}$ pair remains small [42]. This is a result of the saturation of the dipole cross section at smaller dipole size. Under the additional assumption that color fields in distant regions of the large target are uncorrelated, a simple Glauber-type exponentiation of the averaged local field strength results in explicit formulae for all the relevant parton distribution functions [15] (see [43] for a closely related analysis).

Thus, diffractive and inclusive quark and gluon distributions at some small scale Q_0^2 are expressed in terms of only two parameters, the average color field strength and the total size of the large target hadron. The energy dependence arising from the large-momentum cutoff applied in the process of color field averaging can not be calculated from first principles. It is described by a $\ln^2 x$ ansatz, consistent with unitarity, which is universal for

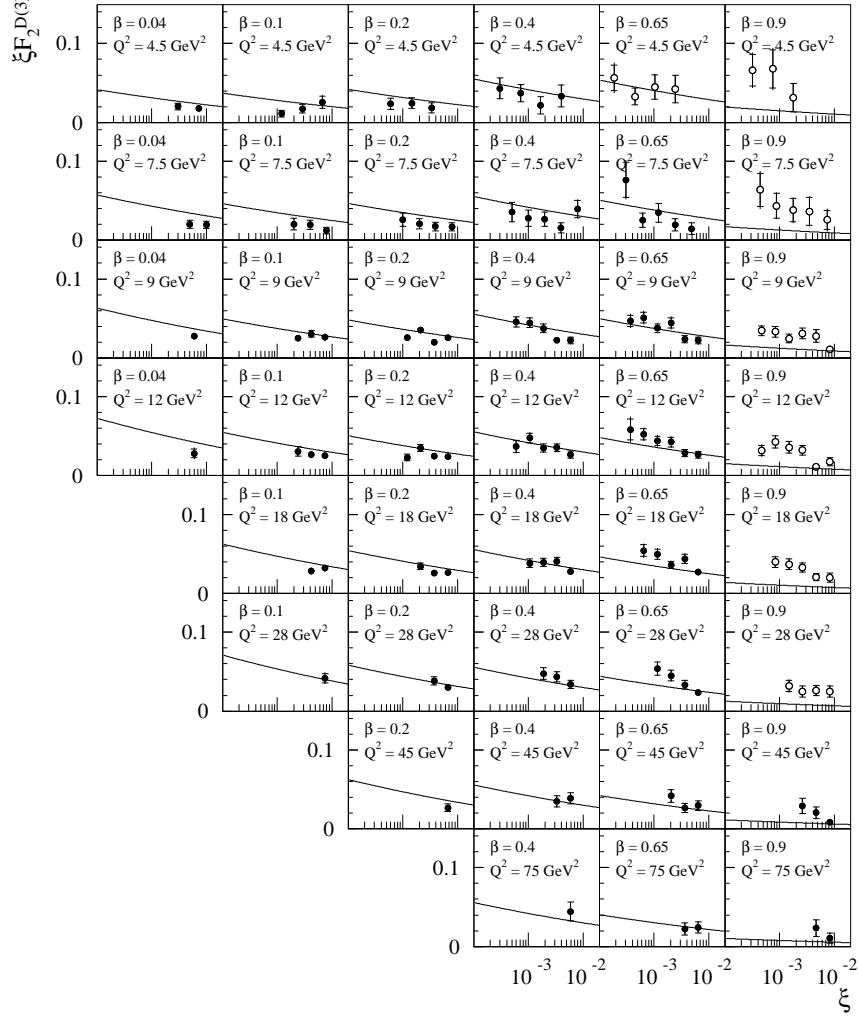


Figure 13: The structure function $F_2^{D(3)}(\xi, \beta, Q^2)$ computed in the semi-classical approach with H1 data from [46]. The open data points correspond to $M^2 \leq 4 \text{ GeV}^2$ and are not included in the fit.

both the inclusive and diffractive structure function [44]. This introduces a further parameter, the unknown constant that comes with the logarithm (see [45] for a related but different way of introducing a phenomenological energy dependence in diffractive and inclusive DIS).

A conventional leading order DGLAP analysis of data at small x and $Q^2 > Q_0^2$ results in a good four parameter fit (Q_0 being the fourth parameter) to both the inclusive and diffractive structure function (Figs. 13 and

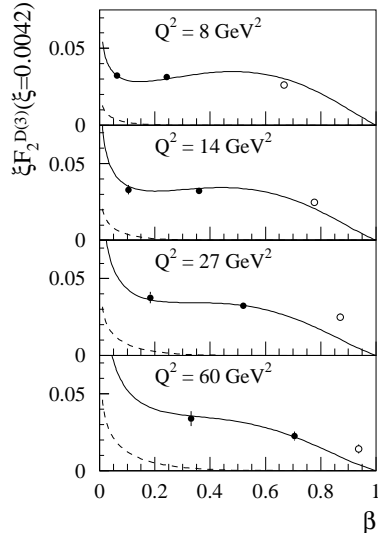


Figure 14: The diffractive structure function $F_2^{D(3)}(\xi, \beta, Q^2)$ with data from ZEUS [47]. Open circles correspond to $M^2 \leq 4 \text{ GeV}^2$. The charm content is indicated as a dashed line.

14). Diffractive data with $M^2 < 4 \text{ GeV}^2$ is excluded from the fit since higher twist effects are expected to affect this region (cf. [24] for a phenomenological discussion of higher twist effects). As an illustration, the β dependence of $F_2^{D(3)}$ at different values of Q^2 is shown in Figs. 13 and 14 (see [15] for further plots, in particular of the inclusive structure function, and more details of the analysis).

Two important qualitative features of the approach should be emphasized. First, the diffractive gluon distribution is much larger than the diffractive quark distribution, a result reflected in the pattern of scaling violations of $F_2^{D(3)}$. This feature is also present in the analysis of [39], where, in contrast to the present approach, the target is modelled as a small color dipole. Second, the inclusive gluon distribution, calculated from $q\bar{q}$ pair production at high p_\perp and determined by the small-distance structure of the color field, is large and leads to the dominance of inclusive over diffractive DIS.

4. Vector meson production

So far, inclusive diffraction, as parametrized, e.g., by the diffractive structure function F_2^D , was at the centre of interest of this review. It was argued that, for inclusive processes, the underlying colour singlet exchange is soft. In perturbative QCD, the simplest possibility of realizing colour singlet exchange is via two t channel gluons. In fact, the colour singlet exchange in

certain more exclusive diffractive processes is, with varying degree of rigour, argued to be governed by a hard scale. In such cases, two-gluon exchange dominates.

4.1. Elastic meson production

Elastic meson electroproduction is the first diffractive process that was claimed to be calculable in perturbative QCD [48, 49]. It has since been considered by many authors, and a fair degree of understanding has been achieved as far as the perturbative calculability and the factorization of the relevant non-perturbative parton distributions and meson wave functions are concerned.

To begin with, consider the electroproduction of a heavy $q\bar{q}$ bound state off a given classical colour field. The relevant amplitude is shown in Fig. 15. In the non-relativistic limit, the two outgoing quarks are on-shell, and each carries half of the J/ψ momentum. Thus, the two quark propagators with momenta $p' = k' = q'/2$ and the J/ψ vertex are replaced with the projection operator $g_J \not{\epsilon}_J (\not{k}' + m)$. Here

$$g_J^2 = \frac{3\Gamma_{ee}^J m_J}{64\pi\alpha_{\text{em}}^2}, \quad (4.1)$$

Γ_{ee}^J is the electronic decay width of the J/ψ particle, $m_J = 2m$ is its mass, and ϵ_J its polarization vector [50].

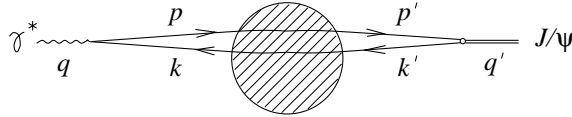


Figure 15: Leading order amplitude for the elastic production of a J/Ψ particle off an external colour field.

Using the calculational technique of Sect. 3.3, the amplitude of Fig. 15 can be expressed in terms of non-Abelian eikonal factors U and U^\dagger associated with the two quarks.

Considering both Q and m as hard scales, while U and U^\dagger are governed by the soft hadronic scale Λ , the integrand in the loop integration of Fig. 15 can be expanded in powers of the soft momentum k_\perp . The leading power of the amplitude is given by the first non-vanishing term. In the case of forward production, $p'_\perp = k'_\perp = 0$, the dependence on the external colour field takes the form [6]

$$\int d^2 k_\perp k_\perp^2 \text{tr} \left[\tilde{U}(p'_\perp - p_\perp) \tilde{U}^\dagger(k_\perp - k'_\perp) - (2\pi)^4 \delta^2(p'_\perp - p_\perp) \delta^2(k'_\perp - k_\perp) \right]$$

$$= -(2\pi)^2 \partial_{y_\perp}^2 \int_{x_\perp} \text{tr} W_{x_\perp}(y_\perp) \Big|_{y_\perp=0} . \quad (4.2)$$

Now, the crucial observation is that precisely the same dependence on the external field is present in the amplitude for forward Compton scattering shown in Fig. 16. In the case of longitudinal photon polarization, the transverse size of the $q\bar{q}$ pair is always small, and the target field enters only via the second derivative of W that appears in Eq. (4.2).

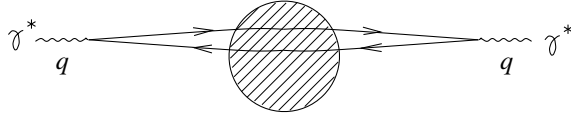


Figure 16: The Compton scattering amplitude within the semiclassical approach.

Thus, comparing with the parton model result for longitudinal photon scattering, this derivative can be identified in terms of the gluon distribution of the target proton [51],

$$-\partial_{y_\perp}^2 \int_{x_\perp} \text{tr} W_{x_\perp}(y_\perp) \Big|_{y_\perp=0} = 2\pi^2 \alpha_s x g(x) . \quad (4.3)$$

Using this relation, the amplitudes for the forward production of transversely and longitudinally polarized J/ψ mesons by transversely and longitudinally polarized virtual photons are obtained. Under the additional assumption $Q^2 \gg m_J^2$, the amplitudes for longitudinal and transverse polarization read

$$T_L = -i64\pi^2 \alpha_s g_J e(xg(x)) \frac{s}{3Q^3} , \quad T_T = \frac{m_J}{Q} T_L , \quad (4.4)$$

where \sqrt{s} is the centre-of-mass energy of the γ^*p collision. This is Ryskin's celebrated result for elastic J/ψ production [48].

It is not surprising that the gluon distribution of Eq. (4.3), calculated according to Fig. 16, shows no scaling violations and only the trivial Bremsstrahlungs energy dependence $\sim 1/x$. The reason for this is the softness assumptions of the semiclassical calculation. Firstly, the eikonal approximation implies that all longitudinal modes of the external field are much softer than the photon energy. Secondly, the reduction of the field dependence to a transverse derivative is only justified if the scales governing the quark loop, i.e., Q^2 in the case of Fig. 16 and Q^2 and m^2 in the case of Fig. 15, are harder than the transverse structure of W . These two

approximations, evidently valid for a given soft field, are also justified for a dynamical target governed by QCD as long as only leading logarithmic accuracy in both $1/x$ and Q^2 is required. Thus, a non-trivial dependence on $1/x$ and Q^2 can be reintroduced into Eq. (4.4) via the measured gluon distribution, keeping in mind that the result is only valid at double-leading-log accuracy.

An essential extension of the above fundamental result is related to the treatment of the bound state produced. Brodsky et al. [49] showed that, at least for longitudinal photon polarization, a perturbative calculation is still possible in the case of light, non-perturbative bound states like the ρ meson. The calculation is based on the concept of the light-cone wave function of this meson (see, however, [53] for an alternative approach to light meson production). Referring the reader to [52] for a detailed review, a brief description of the main ideas involved is given below (cf. [54]). For this purpose, consider the generic diagram for the production of a light meson in a hard QCD process given in Fig. 17.

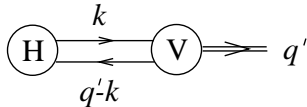


Figure 17: Generic diagram for meson production in a hard process.

Assume that, as shown in this figure, all diagrams can be cut across two quark-lines, the constituent quarks of the meson, in such a way as to separate the hard process H from the soft meson formation vertex V, which is defined to include the propagators. The amplitude can be written as

$$T = \int d^4k T_H(k) V(k) = \int_0^1 dz T_H(z) \frac{q'_+}{2} \int dk_- d^2k_\perp V(k) = \int_0^1 dz T_H(z) \phi(z), \quad (4.5)$$

where $z = k_+/q'_+$, and the last equality is simply the definition of the light-cone wave function ϕ of the meson. The two crucial observations leading to the first of these equalities are the approximate k_- and k_\perp independence of T_H and the restriction of the z integration to the interval from 0 to 1. The first is the result of the hard scale that dominates T_H , the second follows from the analytic structure of V . In QCD, the k_\perp integration implicit in ϕ usually has an UV divergence due to gluon exchange between the quarks. Therefore, one should really read $\phi = \phi(z, \mu^2)$, where the cutoff μ^2 is of the order of the hard scale that governs T_H . At higher orders in α_s , the hard amplitude T_H develops a matching IR cutoff dependence.

The discussion of vector meson production given so far was limited to the double-leading-log approximation as far as the colour singlet exchange

in the t channel is concerned. To go beyond this approximation, the concept of ‘non-forward’ or ‘off-diagonal’ parton distributions, introduced some time ago (see [55] and refs. therein) and discussed by Ji [56] and Radyushkin [57] in the present context, has to be used (see also [58]).

Recall first that the semiclassical viewpoint of Figs. 15 and 16 is equivalent to two-gluon exchange as long as the transverse size of the energetic $q\bar{q}$ state is small. So far, the recoil of the target in longitudinal direction has been neglected. However, such a recoil is evidently required by the kinematics. For what follows, it is convenient to use a frame where q_- is the large component of the photon momentum. In Fig. 18, the exchanged gluons and the incoming and outgoing proton with momenta P and P' are labelled by their respective fractions of the plus component of $\bar{P} \equiv (P + P')/2$. If Δ is the momentum transferred by the proton, $\xi\bar{P}_+ = \Delta_+/2$. The variable y is an integration variable in the gluon loop.

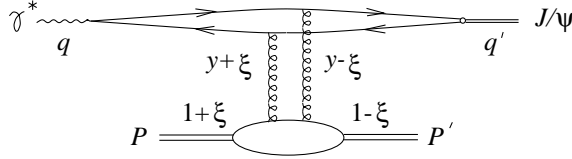


Figure 18: Elastic J/ψ production (three further diagrams with the gluons connected in different ways have to be added). The two gluon lines and the incoming and outgoing proton are labelled by their respective fractions of the plus component of $\bar{P} \equiv (P + P')/2$.

The lower part of the diagram in Fig. 18 is a generalization of the conventional gluon distribution. It can be described by the non-forward gluon distribution

$$H_g(y, \xi, t) = \frac{1}{4\pi y \bar{P}_+} \int dx_- e^{-iy\bar{P}_+ x_- / 2} \langle P' | F^\dagger(0, x_-, 0_\perp)^{+\mu} F(0, 0, 0_\perp)_\mu^+ | P \rangle. \quad (4.6)$$

The description of elastic meson production in terms of non-forward parton distributions is superior to the double-leading-log approach of [48, 49] since α_s corrections to the hard amplitude, meson wave function and parton distribution function can, at least in principle, be systematically calculated. However, the direct relation to the measured conventional gluon distribution is lost. A new non-perturbative quantity, the non-forward gluon distribution, is introduced, which has to be measured and the evolution of which has to be tested – a very complicated problem given the uncertainties of the experiment and of the meson wave functions involved (see [59] for possibilities of predicting the non-forward from the forward distribution functions).

4.2. Factorization

Having discussed the leading order results for vector meson production, the next logical step is to ask whether the systematic calculation of higher order corrections is feasible. For this, it is necessary to understand the factorization properties of the hard amplitude and the two non-perturbative objects involved, i.e., the meson wave function and the non-forward gluon distribution.

Factorization means that, to leading order in $1/Q$, the amplitude can be written as

$$T = \int_0^1 dz \int dy H(y, x/2) T_H(Q^2, y/x, z, \mu^2) \phi(z, \mu^2), \quad (4.7)$$

where T_H is the hard scattering amplitude, ϕ is the light-cone wave function of the vector meson produced, and H is the non-forward parton distribution of the proton. It could, for example, be the non-forward gluon distribution H_g of the last section. The variable $x = x_{\text{Bj}}$ is the usual DIS Bjorken variable.

In these notes, I will not describe the factorization proof for longitudinal vector meson production given in [60]. Instead, a particularly simple situation will be used to show how factorization works specifically at small x , from the point of view of the target rest frame [61]. For this purpose, consider a very energetic scalar photon that scatters off a hadronic target producing a scalar meson built from two scalar quarks (see Fig. 19). The quarks are coupled to the photon and the meson by point-like scalar vertices ie and $i\lambda$, where e and λ have dimension of mass. The coupling of the gluons to the scalar quarks is given by $-ig(r_\mu + r'_\mu)$, where r and r' are the momenta of the directed quark lines, and g is the strong gauge coupling.

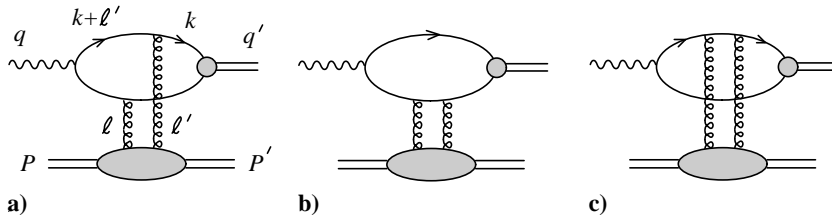


Figure 19: The leading amplitude for a point-like meson vertex.

Under quite general conditions [61], the gluon momenta satisfy the relations $l_+, l'_+ \ll q_+, l_-, l'_- \ll P_-$ and $l_\perp^2 \sim l'^2 \sim -l_\perp^2$. Then the lower bubble in Fig. 19 effectively has the structure

$$F^{\mu\nu}(\ell, \ell', P) \simeq \delta(P_- \ell_+) F(\ell_\perp^2) P^\mu P^\nu, \quad (4.8)$$

which is defined to include both gluon propagators and all colour factors.

Assume that F restricts the gluon momentum to be soft, $\ell_\perp^2 \ll Q^2$. In the high-energy limit, it suffices to calculate

$$M = \int \frac{d^4\ell}{(2\pi)^4} T^{\mu\nu} F_{\mu\nu} \simeq \int \frac{d^4\ell}{4(2\pi)^4} T_{++} F_{--}, \quad (4.9)$$

where

$$T^{\mu\nu} = T^{\mu\nu}(\ell, \ell', q) = T_a^{\mu\nu} + T_b^{\mu\nu} + T_c^{\mu\nu} \quad (4.10)$$

is the sum of the upper parts of the diagrams in Fig. 19.

Note that, because of the symmetry of $F_{\mu\nu}$ with respect to the two gluon lines, the amplitude $T^{\mu\nu}$ of Eq. (4.10) is used instead of the properly-symmetrized upper amplitude

$$T_{\text{sym}}^{\mu\nu}(\ell, \ell', q) = \frac{1}{2} [T^{\mu\nu}(\ell, \ell', q) + T^{\nu\mu}(-\ell', -\ell, q)]. \quad (4.11)$$

The two exchanged gluons together form a colour singlet and so the symmetrized amplitude $T_{\text{sym}}^{\mu\nu}$ satisfies the same Ward identity as for two photons,

$$T_{\text{sym}}^{\mu\nu}(\ell, \ell', q) \ell_\mu \ell'_\nu = 0. \quad (4.12)$$

Writing this equation in light-cone components and setting $\ell_\perp = \ell'_\perp$, as appropriate for forward production, it follows that, for the relevant small values of ℓ_- , ℓ'_- , ℓ_+ and ℓ'_+ ,

$$T_{\text{sym},++} \sim \ell_\perp^2 \quad (4.13)$$

in the limit $\ell_\perp^2 \rightarrow 0$. Here the fact that the tensor $T_{\text{sym}}^{\mu\nu}$, which is built from ℓ' , ℓ and q , has no large minus components has been used. The ℓ_- integration makes this equation hold also for the original, unsymmetrized amplitude,

$$\int d\ell_- T_{++} \sim \ell_\perp^2. \quad (4.14)$$

This is the crucial feature of the two-gluon amplitude that will simplify the calculation and lead to the factorizing result below.

Consider first the contribution from diagram a) of Fig. 19 to the ℓ_- integral of T_{++} , which is required in Eq. (4.9),

$$\int d\ell_- T_{a,++} = -4eg^2q_+ \int \frac{d^4k}{(2\pi)^3} \frac{z(1-z)}{N^2 + (k_\perp + \ell_\perp)^2} \frac{i\lambda}{k^2(q' - k)^2}. \quad (4.15)$$

Here $N^2 = z(1-z)Q^2$, $z = k_+/q_+$ and the condition $\ell_+ = 0$, enforced by the δ -function in Eq. (4.8), has been anticipated.

Now $\int d\ell_{-} T_{b,++}$ and $\int d\ell_{-} T_{c,++}$ each carry no ℓ_{\perp} dependence. So, to ensure the validity of Eq. (4.14), the sum of the three diagrams must be

$$\int d\ell_{-} T_{++} = 4eg^2 q_+ \int \frac{d^4 k}{(2\pi)^3} z(1-z) \mathcal{N} \frac{i\lambda}{k^2(q'-k)^2}, \quad (4.16)$$

where

$$\mathcal{N} = \left[\frac{1}{N^2 + k_{\perp}^2} - \frac{1}{N^2 + (k_{\perp} + \ell_{\perp})^2} \right] \sim \frac{\ell_{\perp}^2}{(N^2 + k_{\perp}^2)^2}. \quad (4.17)$$

Note the $1/Q^4$ behaviour obtained after a cancellation of $1/Q^2$ contributions from the individual diagrams. This cancellation is closely related to the well-known effect of colour transparency.

Introduce the k_{\perp} dependent light-cone wave function of the meson

$$\phi(z, k_{\perp}^2) = -\frac{iq'_+}{2} \int dk_{-} dk_+ \frac{i\lambda}{(2\pi)^4 k^2 (q' - k)^2} \delta(k_+ - zq'_+). \quad (4.18)$$

The final result following from Eqs. (4.9) and (4.16) is a convolution of the production amplitude of two on-shell quarks and the light-cone wave function:

$$M = ieg^2 s \left(\int \frac{d^2 \ell_{\perp}}{2(2\pi)^3} \ell_{\perp}^2 F(\ell_{\perp}^2) \right) \int dz \int d^2 k_{\perp} \frac{z(1-z)}{(N^2 + k_{\perp}^2)^2} \phi(z, k_{\perp}^2). \quad (4.19)$$

This corresponds to the $O(\ell_{\perp}^2)$ term in the Taylor expansion of the contribution from Fig. 19a, given in Eq. (4.15).

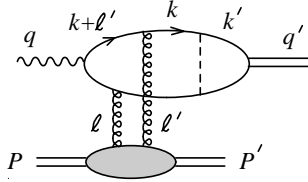


Figure 20: Diagram for meson production with the vertex modelled by scalar particle exchange.

At leading order, factorization of the meson wave function was trivial since the point-like quark-quark-meson vertex $V(k^2, (q' - k)^2) = i\lambda$ was necessarily located to the right of the all other interactions. To see how

factorization comes about in the simplest non-trivial situation, consider the vector meson vertex

$$V(k^2, (q' - k)^2) = \int \frac{d^4 k'}{(2\pi)^4} \frac{i\lambda\lambda'^2}{k'^2(q' - k')^2(k - k')^2}, \quad (4.20)$$

which corresponds to the triangle on the r.h. side of Fig. 20. Here, the dashed line denotes a colourless scalar coupled to the scalar quarks with coupling strength λ' .

The diagram of Fig. 20 by itself gives no consistent description of meson production since it lacks gauge invariance. This problem is not cured by just adding the two diagrams 19b) and c) with the blob replaced by the vertex V . It is necessary to include all the diagrams shown in Fig. 21.

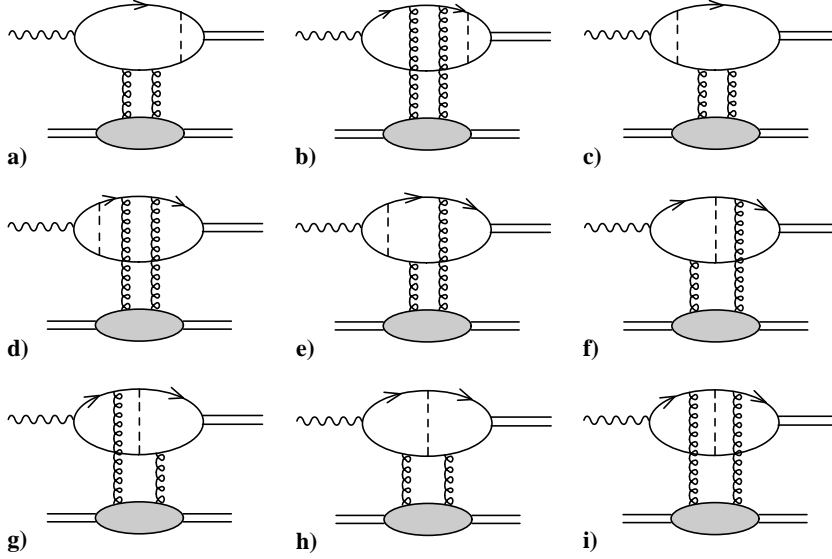


Figure 21: The remaining diagrams contributing to meson production within the above simple model for the meson wave function.

The same gauge invariance arguments that lead to Eq. (4.14) apply to the sum of all the diagrams in Figs. 20 and 21. Therefore, the complete result for T_{++} , which is now defined by the sum of the upper parts of all these diagrams, can be obtained by extracting the ℓ_{\perp}^2 term at leading order in the energy and Q^2 . Such a term, with a power behaviour $\sim \ell_{\perp}^2/Q^4$, is obtained from the diagram in Fig. 20 (replace $i\lambda$ in Eq. (4.15) with the vertex V of Eq. (4.20)) by expanding around $\ell_{\perp} = 0$. It can be demonstrated that none of the other diagrams gives rise to such a leading-order ℓ_{\perp}^2 contribution (see [61] for more details).

The complete answer is given by the ℓ_{\perp}^2 term from the Taylor expansion of Eq. (4.15). The amplitude M is precisely the one of Eqs. (4.19) and (4.18), with $i\lambda$ substituted by V of Eq. (4.20). The correctness of this simple factorizing result has also been checked by explicitly calculating all diagrams of Fig. 21.

The above simple model calculation can be summarized as follows. The complete result contains leading contributions from diagrams that cannot be factorized into quark-pair production and meson formation. However, the answer to the calculation can be anticipated by looking only at one particular factorizing diagram. The reason for this simplification is gauge invariance. In the dominant region, where the transverse momentum ℓ_{\perp} of the two t -channel gluons is small, gauge invariance requires the complete quark part of the amplitude to be proportional to ℓ_{\perp}^2 . The leading ℓ_{\perp}^2 dependence comes exclusively from one diagram. Thus, the complete answer can be obtained from this particular diagram, which has the property of factorizing explicitly if the two quark lines are cut. The resulting amplitude can be written in a factorized form.

Note finally that, although QCD predicts factorization for longitudinal vector meson production and a $1/Q^2$ suppression of the transverse cross section, this behaviour is not visible in the data [62]. A recent calculation [63] explaining the data is, in my opinion, in conflict with QCD expectations and, in particular, with the implications of [61], since it employs a non-local vector meson vertex in a loop calculation. It is important to clarify this situation.

5. Summary

The phenomenon of diffraction in DIS can be understood in very simple terms if the process is viewed in the rest frame of the target proton. The energetic virtual photon develops a partonic fluctuation which then scatters off the target. A certain fraction of the total DIS cross section is due to photon fluctuations with large transverse size. This fraction is not power suppressed in the high- Q^2 limit. Since, as one expects from the experience with hadron-hadron collisions, part of these large size fluctuations scatter quasi-elastically off the proton, a leading twist diffractive cross section is obtained.

One possibility to describe the interaction of the photon fluctuation with the target is two-gluon exchange. In certain more exclusive processes, such as longitudinally polarized vector meson production, the transverse size of the relevant photon fluctuations is always small and two-gluon calculations can be rigorously justified. However, for most of the diffractive cross section no suppression of multiple gluon exchange can be derived.

This problem is addressed in the semiclassical approach, where the target is described by a superposition of soft colour fields and gluon exchange is resummed to all orders in an eikonal approximation. Diffraction arises whenever the partonic fluctuation of the photon remains in a colour singlet. The application of the semiclassical approach to experimental results is particularly simple if the approach is used to derive both diffractive and inclusive parton distributions at some small input scale. In this case, the analysis of all higher- Q^2 data proceeds with standard perturbative methods. Different models for the underlying colour fields can be compared to diffractive and inclusive structure function data in a very direct way.

Acknowledgements

I have greatly benefited from my work with W. Buchmüller, M.F. McDermott and T. Gehrmann, the results of which are reflected in part of these notes. I would also like to thank the organizers of the XXXIXth Cracow Summer School for their invitation and their warm hospitality.

REFERENCES

- [1] M.L. Good and W.D. Walker, Phys. Rev. 120 (1960) 1857
- [2] UA8 collab., A. Brandt et al., Phys. Lett. B297 (1992) 417
- [3] M. Derrick, *these proceedings*
- [4] ZEUS collab., M. Derrick et al., Phys. Lett. B315 (1993) 481
- [5] H1 collab., T. Ahmed et al., Nucl. Phys. B429 (1994) 477
- [6] A. Hebecker, preprint HD-THEP-99-12 (hep-ph/9905226)
- [7] B. Andersson et al., Phys. Rep. 97 (1983) 31
- [8] A. Edin, G. Ingelman and J. Rathsman, Phys. Lett. B366 (1996) 371;
J. Rathsman, Phys. Lett. B452 (1999) 364
- [9] G. Ingelman and K. Jansson-Prytz, Proc. of the Workshop *Physics at HERA*, Hamburg 1991, Ed. W. Buchmüller and G. Ingelman;
G. Ingelman and K. Prytz, Z. Phys. C58 (1993) 285
- [10] H1 collab., T. Ahmed et al., Phys. Lett. B348 (1995) 681
- [11] W. Buchmüller, talk at *New Trends in HERA Physics*, Ringberg Workshop 1999 (hep-ph/9906546)
- [12] J.D. Bjorken and J.B. Kogut, Phys. Rev. D8 (1973) 1341
- [13] N.N. Nikolaev and B.G. Zakharov, Z. Phys. C49 (1991) 607
- [14] W. Buchmüller and A. Hebecker, Nucl. Phys. B476 (1996) 203;
W. Buchmüller, M.F. McDermott and A. Hebecker, Nucl. Phys. B487 (1997) 283; B500 (1997) 621 (E)
- [15] W. Buchmüller, T. Gehrmann and A. Hebecker, Nucl. Phys. B537 (1999) 477

- [16] G. Ingelman and P. Schlein, Phys. Lett. B152 (1985) 256
- [17] A. Donnachie and P.V. Landshoff, Phys. Lett. B191 (1987) 309
- [18] L. Trentadue and G. Veneziano, Phys. Lett. B323 (1994) 201
- [19] A. Berera and D.E. Soper, Phys. Rev. D50 (1994) 4328
- [20] M. Wüsthoff and A.D. Martin, preprint DTP-99-78 (hep-ph/9909362)
- [21] N.N. Nikolaev and B.G. Zakharov, Z. Phys. C64 (1994) 631
- [22] J. Bartels and M. Wüsthoff, Z. Phys. C66 (1995) 157;
M. Wüsthoff, Phys. Rev. D56 (1997) 4311
- [23] S.J. Brodsky, P. Hoyer and L. Magnea, Phys. Rev. D55 (1997) 5585
- [24] J. Bartels et al., Eur. Phys. J. C7 (1999) 443
- [25] G. Salam, *these proceedings*
- [26] M. Genovese, N.N. Nikolaev and B.G. Zakharov, JETP 81 (1995) 625;
A. Bialas and R. Peschanski, Phys. Lett. B387 (1996) 405
- [27] A. Bialas, R. Peschanski and C. Royon, Phys. Rev. D57 (1998) 6899
- [28] O. Nachtmann, Ann. Phys. 209 (1991) 436
- [29] J. D. Bjorken, J. Kogut and D. E. Soper, Phys. Rev. D3 (1971) 1382
- [30] J.C. Collins, D.E. Soper and G. Sterman, Nucl. Phys. B263 (1986) 37
- [31] A. Berera and D.E. Soper, Phys. Rev. D53 (1996) 6162
- [32] J.C. Collins, D.E. Soper and G. Sterman, in *Perturbative QCD*, Ed. A.H. Mueller, World Scientific, Singapore, 1989, p. 1
- [33] M. Grazzini, L. Trentadue and G. Veneziano, Nucl. Phys. B519 (1998) 394
- [34] J.C. Collins, Phys. Rev. D57 (1998) 3051
- [35] A. Capella et al., Phys. Lett. B343 (1995) 403;
B.A. Kniehl, H.-G. Kohrs and G. Kramer, Z. Phys. C65 (1995) 657;
K. Golec-Biernat and J. Kwieciński, Phys. Lett. B353 (1995) 329;
T. Gehrmann and W.J. Stirling, Z. Phys. C70 (1996) 89
- [36] A. Donnachie and P.V. Landshoff, Nucl. Phys. B244 (1984) 322 and Phys. Lett. B296 (1992) 227
- [37] A. Hebecker, Nucl. Phys. B505 (1997) 349
- [38] H.G. Dosch, A. Krämer, Phys. Lett. B252 (1990) 669;
H.G. Dosch, E. Ferreira and A. Krämer, Phys. Rev. D50 (1994) 1992;
H.G. Dosch, *these proceedings*
- [39] F. Hautmann, Z. Kunszt and D.E. Soper, Phys. Rev. Lett. 81 (1998) 3333
and preprint CERN-TH/99-154 (hep-ph/9906284)
- [40] L. McLerran and R. Venugopalan, Phys. Rev. D49 (1994) 2233
- [41] L. McLerran, *these proceedings*;
R. Venugopalan, *these proceedings*
- [42] A. Hebecker and H. Weigert, Phys. Lett. B432 (1998) 215
- [43] Yu.V. Kovchegov and L. McLerran, Phys. Rev. D60 (1999) 054025
- [44] W. Buchmüller, Phys. Lett. B353 (1995) 335

- [45] K. Golec-Biernat and M. Wüsthoff, preprint DTP/99/20 (hep-ph/9903358)
- [46] H1 collab., C. Adloff et al., *Z. Phys.* C76 (1997) 613
- [47] ZEUS collab., J. Breitweg et al., *Eur. Phys. J.* C6 (1999) 43
- [48] M.G. Ryskin, *Z. Phys.* C57 (1993) 89
- [49] S.J. Brodsky et al., *Phys. Rev.* D50 (1994) 3134
- [50] E.L. Berger and D. Jones, *Phys. Rev.* D23 (1981) 1521
- [51] W. Buchmüller, M.F. McDermott and A. Hebecker, *Phys. Lett.* B410 (1997) 304
- [52] V.L. Chernyak and A.R. Zhitnitsky, *Phys. Rep.* 112 (1984) 173
- [53] A.D. Martin, M.G. Ryskin and T. Teubner, *Phys. Rev.* D55 (1997) 4329
- [54] B. Pire, Lectures at *Les Houches Summer School 1996: Trends in Nuclear Physics* (nucl-th/9612009)
- [55] F.-M. Dittes et al., *Phys. Lett.* B209 (1988) 325;
D. Müller et al., *Fortsch. Phys.* 42 (1994) 101
- [56] X. Ji, *Phys. Rev. Lett.* 78 (1997) 610
- [57] A.V. Radyushkin, *Phys. Lett.* B380 (1996) 417
- [58] A.V. Radyushkin, *Phys. Rev.* D56 (1997) 5524;
X. Ji, *J. Phys.* G24 (1998) 1181;
K.J. Golec-Biernat and A.D. Martin, *Phys. Rev.* D59 (1999) 014029;
A.V. Radyushkin, *these proceedings*
- [59] A.G. Shuvaev et al., *Phys. Rev.* D60 (1999) 014015;
K.J. Golec-Biernat, A.D. Martin and M.G. Ryskin, *Phys. Lett.* B456 (1999) 232
- [60] J.C. Collins, L. Frankfurt and M. Strikman, *Phys. Rev.* D56 (1997) 2982
- [61] A. Hebecker and P.V. Landshoff, *Phys. Lett.* B419 (1998) 393
- [62] ZEUS collab., J. Breitweg et al., *Eur. Phys. J.* C6 (1999) 603;
H1 collab., C. Adloff et al., preprint DESY-99-010 (hep-ex/9902019)
- [63] I. Royen and J.R. Cudell, *Nucl. Phys.* B545 (1999) 505